3D finite modeling of the blow molding process

Cédric Champin, Michel Bellet, Fabrice Schmidt, Jean François Agassant, Yannick Le Maoult

3D finite element modeling of the blow molding process

C. Champin[1,2], M. Bellet[1], F.M. Schmidt[2], J.-F. Agassant[1], Y. Le Maoult[2]

[1]*Ecole des Mines de Paris - CEMEF – BP207 F-06904 SOPHIA ANTIPOLIS Cedex*
e-mail: cedric.champin@ensmp.fr; michel.bellet@ensmp.fr; jean-francois.agassant@ensmp.fr

[2]*Ecole des Mines d'Albi - CROMeP – F-81013 ALBI Cedex 09*
e-mail: fabrice.schmidt@enstimac.fr; yannick.lemaoult@enstimac.fr

ABSTRACT: In this work, both the heating stage and the blowing stage of the blow molding process are numerically modeled. The heat transfer between the infrared oven and the preform is modeled using a ray tracing method. The cooling fan effect is taken into account thanks to a forced convection coefficient. Regarding the blowing step, a Mooney-Rivlin hyperelastic model has been implemented in Forge3® software in order to account for the rheological behavior of the polyester. The finite element model is based on velocity pressure formulation and tetrahedral elements. In order to validate the implementation of the hyperelastic behavior, computations are compared to Mooney-Rivlin analytical model results for tube free inflation. Finally, the global blow molding process of a PET bottle is studied.

Key words: Blow molding modeling, hyperelasticity, radiation, ray tracing.

1 INTRODUCTION

The injection stretch-blow molding process is the most widely used in PET bottle production [1]. This process is segmented in two main stages. First, a cold preform is heated in an infrared oven above glass transition temperature (~80°C). Then, the softened preform is inflated and stretched with assistance of a rod in a mold which has the shape of the desired bottle.

A few heat transfer models in an infrared oven have been developed [2,3]. In 1993, DiRaddo et al [4] proposed a 2D finite element model where the fraction of energy leaving the lamp surface and reaching at the preform surface (view factor) is estimated analytically. Hartwig [5] included the influence of back and front reflectors and the displacement of the preform in the oven. Monteix carried out numerical simulations of the temperature distribution of preform using control-volum method and compared it with experimental data [6].

The blowing step has been also the subject of significant researches within the last two decades [7,8]. But must of the papers use a hyperelastic behavior based on Mooney-Rivlin or neo-Hookean potentials. Queen's University of Belfast has programmed a special Abaqus® version dedicated to the blow molding simulation using Mooney-Rivlin, Ogden or Buckley hyperelastic laws [9]. Recently, Gorlier [10] or Marco [11] pointed out that the Edwards Vilgis potential [12] allows to capture the deformation of PET subjected to multi-axial loads. Moreover, the thin shell models reach their limits regarding the more and more complex bottle shapes.

As a consequence, the two steps of the stretch blow molding process will be computed in this work with a 3D finite element model implemented in the Forge3® commercial software. First, a modeling approach capable of predicting the three-dimensional transient temperature profile in the preform during the conditioning step is presented, taking into account conduction, convection and radiation. The mechanical problem is considered using Newtonian or hyperelastic Mooney-Rivlin laws implemented with a velocity/pressure formulation.

2 INFRARED HEATING MODEL

In its classical form, the heat balance equation can be written :

$$\rho c_p \frac{dT}{dt} = \nabla \cdot (k \nabla T) - \nabla \cdot \left(\dot{q_r} \right) \qquad (1)$$

Notations are detailed in the nomenclature at the end of the paper. To calculate the density radiative heat flux, a ray tracing method coupled with a Beer-Lambert approximation has been implemented. It allows to calculate with accuracy the absorption of the radiation inside the material. Along each ray emitted, the Beer-Lambert law can be applied :

$$\vec{q_r} = q_0 e^{-\bar{A}l} \vec{d} \qquad (2)$$

The intensity of radiation emitted by a lamp at 2415K is about $L = 1.66 \times 10^5$ $Wsr^{-1}m^{-2}$ [13]. As a consequence, the emissive power of radiation for each beam can be calculated :

$$q_0 = \frac{pLS_W}{Nbr\ beams S_{Elt}} \quad (3)$$

The energy absorbed inside the material depends on the average absorption coefficient which can be determined using the Planck function and the measured value of the spectral absorption coefficient

$$\overline{A} = \frac{\int_{\Delta l} A_l L_l^0(T) dl}{\int_{\Delta l} L_l^0(T) dl} \quad (4)$$

The halogen lamp is modeled by its tungsten filament and its ceramic reflector. For each surface node, a constant number of emitted rays is defined. The orientation and the energy of each ray is defined in order to get an isotropic radiation in the half space determined by the outward normal vector.

In a first step, to calculate the interception between a ray and the preform heated, a three equations with three unknowns system is solved considering the beam equation and the boundary element area of the preform. If the beam intercepts first the back reflector, its direction is recalculated considering a specular reflexion and tested again with the object. In a second step, the ray's trajectory and the heat flux absorbed are defined using the connectivity of the mesh and the Beer-Lambert approximation.

The irradiance calculation has been validated comparing the Forge3® results with an analytical model of an element on plane facing a cylinder [14]. As shown in figure 1, the agreement is fair (about 10%).

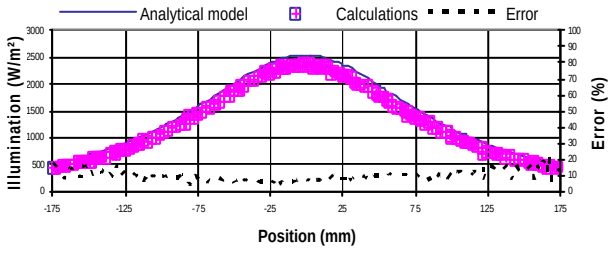

Fig. 1. Irradiance of a plate (350 x 350 mm), 100mm distance from a lamp (350 mm length / 0.81 mm diameter).

The calculation of the amount of energy received by the plate is validated using Philips measurement [13]. Like the comparison with the analytical model, the final error is about 10% (figure 2).

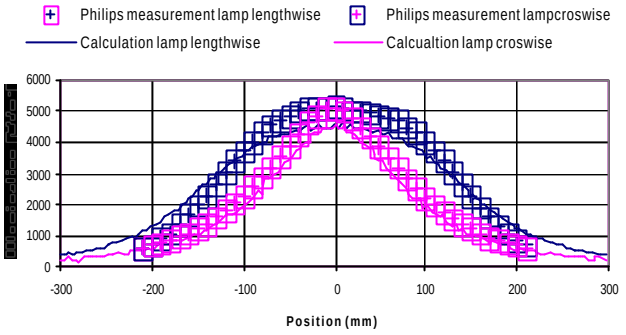

Fig. 2. Irradiance of a plate (600 x 600 mm), 100 mm distance from a lamp (280 mm length / 2.15 mm diameter)

Finally, the temperature evolution in the preform heated with one lamp (figure 3) or with six lamps (figure 4) is obtained, taking into account the natural convection and the ceramic reflector of the lamp.

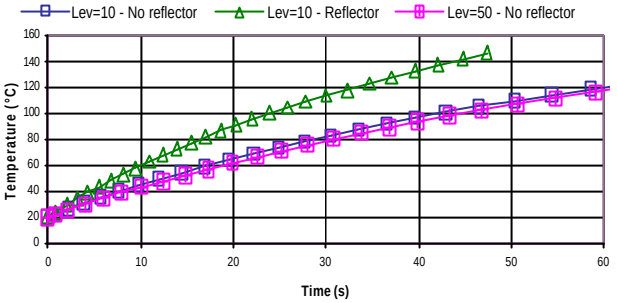

Fig. 3. Surface temperature versus time at mid-height of the preform depending on number of beams and back reflector.

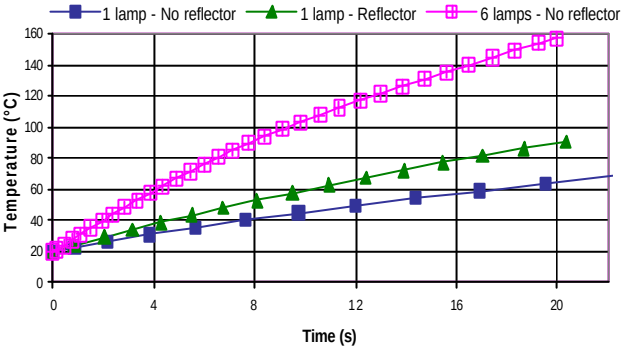

Fig. 4. Surface temperature versus time at mid-height of the preform depending on number of lamps.

3 MECHANICAL MODEL

As shown by many authors [10-11], the PET exhibits a hyperelastic rheological behavior above its glass transition temperature. Assuming incompressibility and Mooney-Rivlin potential, the expression of the Cauchy stress tensor is [15] :

$$\underline{\underline{s}} = -p' \underline{\underline{I}} + \underline{\underline{s}}' = -p' \underline{\underline{I}} + 2C\underline{\underline{B}} - 2Ca\,\underline{\underline{B}}^{-1} \quad (5)$$

This rheological model has been implemented in Forge3® using a velocity/pressure updated Lagrangian formulation together with P1+/P1 tetrahedral finite elements.

This results in a set of non linear equations, the unknown of which are the nodal velocity field and the nodal pressure field. This set of equations is solved by a Newton-Raphson method. For validation purpose, an analytical solution has been developed [16] in an axi-symmetric thick tube inflated with an imposed internal pressure. The lower and upper sections of the tube are supposed to slip freely along fixed horizontal planes. The polymeric tube is assumed to have a Mooney-Rivlin behavior. In figure 5, both numerical and analytical internal radius versus pressure are plotted as well as error. The agreement is fair (maximum error 4%).

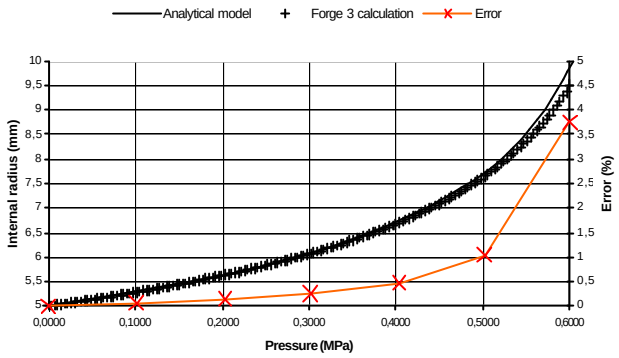

Fig. 5. Internal radius variation versus pressure.

4 BLOWING MODEL

An isothermal free inflation simulation of a preform has been performed using a neo-Hookean behavior ($a = 0$ in equation (5)). The parameters used for this calculation have been referenced in table 1.

Table1. Calculation parameters.

Neo-Hookean parameters	C = 1 Mpa a = 0
Pressure ramps	Linear t = 0 s ⟶ P = 0 MPa t = 0.8 s ⟶ P = 0.8 MPa
Preform dimensions	Thickness = 3 mm Internal radius = 10 mm Length = 101 mm

Figure 6 presents successive steps of the free blow molding process.

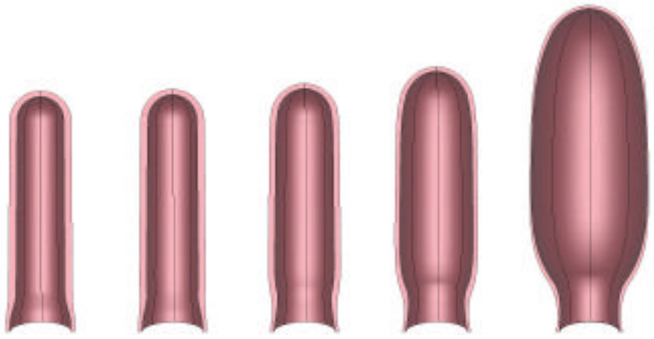

$t = 0\ s$ $t = 0.2\ s$ $t = 0.4\ s$ $t = 0.6\ s$ $t = 0.8\ s$

Fig. 6. Successive configurations during free inflation.

Moreover, the relaxation phase due to the hyperelastic behavior can be checked numerically : if the pressure applied inside the preform decreases to zero, then, the preform relaxes to its initial shape.

As a second example, a confined blow molding simulation (without rod) has been done. We assume an isothermal Newtonian law behavior. The mould used is a prototype one developed at CROMeP (table 2). It produces 50 cl water bottle.

Table2. Calculation parameters.

Newtonian viscosity	h = 0.2 Mpa s
Pressure ramp	Linear t = 0 s ⟶ P = 0 MPa t = 1 s ⟶ P = 1 MPa
Preform dimensions	Thickness = 2.35 mm Internal radius = 7.6 mm Length = 68.5 mm
Mold dimensions	Internal radius = 64 mm Length of the print = 119 mm

As for the tube inflation, just one eighth of the preform has been meshed (figure 7).

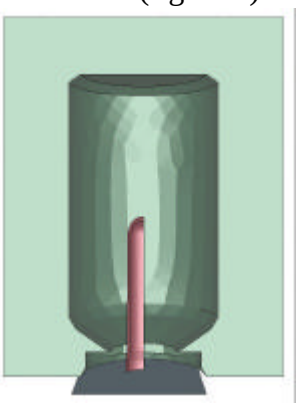

Fig. 7. Geometries of the preform and the mold.

Figure 8 shows the inflation of the preform as a function of time and especially the development of the contact between polymer and mold.

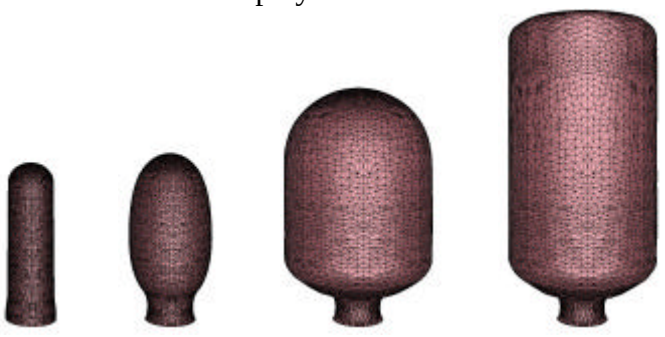

$t = 0\ s$ $t = 0.4\ s$ $t = 0.5\ s$ $t = 0.6\ s$

Fig. 8. Successive configurations during blow molding.

5 CONCLUSION AND PROSPECTS

A numerical thermo-mechanical model has been developed using Forge3® velocity/pressure formulation and tetrahedral elements. From a

thermal point of view, a ray tracing method coupled with a Beer-Lambert approximation has been implemented. This method has been compared with an analytical model of view factor calculations and irradiance measurement on a plate. Ceramic reflector and tungsten filament have been modeled. The calculations confirm the major role of the back reflector on each lamp. From a mechanical point of view, a Mooney-Rivlin hyperelastic behavior law has been implemented with a finite element formulation including consistent tangent stiffness terms. The model has been validated by comparison with an analytical calculation of tube inflation.

Future work will consist in testing alternative hyperelastic potentials and modeling the stretch step in order to compare the final thickness distribution with experimental data.

ACKNOWLEDGEMENT

This study has been supported by Nestlé Waters Management & Technology (PTC Vittel). Special thanks go to G. Denis, K. Hartwig and C. Boulay for their help in this work.

REFERENCES

1. D. Rosato, *Blow molding handbook*, Hanser Pub. (1989).
2. P. Lebaudy, J.M. Saiter, J. Grenet, C. Vautier, Temperature distribution in poly(ethylene terephtalate) plate undergoing heat treatment, Diffusion influence : 1, Theoretical approach. *Polymer*. 33 n°9 (1992) 1887-1892.
3. M.D. Shelby, Effects of infrared lamp temperature and other variable on the reheat rate of PET. *ANTEC* (1991).
4. R. DiRaddo, A. Garcia-Rejon, Dynamic modeling of the preform reheating stage in injection blow molding. *Plastic Rubber and composites processing and applications*. 20 n°5 (1993).
5. K. Hartwig, Simulation of the stretch blow molding process and characterisation of the relevant material behaviour. *Ph. D. Dissertation*. RWTH, Aachen (1996).
6. S. Monteix, F. Schmidt, Y. Le Maoult, R. Ben Yedder, R.W. Diraddo, D. Laroche, Experimental study and numerical simulation of preform or sheet exposed to infrared radiative heating. *Journal of Materials Processing Technology*. 119 (2001) 90-97.
7. F. Schmidt, J.F. Agassant, M. Bellet, G. Denis, Numerical simulation of polyester stretch-blow molding. *Numerical methods in industrial forming processes*, Balkema, Rotterdam (1992) 383.
8. S. Wang, A. Makinouchi, T. Nakagawa, 3D viscoplastic FEM simulation of a stretch blow molding process. *International Journal for Numerical Methods in Engineering*. 48 n°4 (2000) 501-521.
9. G.H. Menary, C.G. Armonstrong, R.J. Crawford and J.P. McEvoy, Modeling of Poly(ethylene terephtalate) in injection stretch blow molding. *Plastics, Rubber and Composites*. 29 n°7 (2000) 360-370.
10. E. Gorlier, J.F. Agassant, J.M. Haudin, N.Billon, Experimental and theoretical study of uniaxial deformation of amorphous P.E.T. above glass transition temperature. *Plastics, Rubber and Composites*. 30 (2001) 48-55.
11. Y. Marco, Caractérisation multi-axiale du comportement et de la micro-structure d'un semi-cristallin : application au cas du P.E.T. *Ph.D. Dissertation*. Ecole Normale Supérieure de Cachan. In french (2003).
12. S.F. Edwards, T. Vilgis, The effect of entanglements in rubber elasticity. *Polymer*. 27 (1986) 483-492.
13. M. Bordival, Training period report, Ecole des Mines d'Abli Carmaux. In french (2004).
14. H. Leuenberger and R.A. Person, Compilation of radiation shape factors for cylindrical assemblies. *ASME*, paper no. 56-A-144, November (1956).
15. P. Germain, *Cours de Mécanique des Milieux Continus*. Tome 1, Théorie Générale, Masson et Cie editeurs. In french (1973).
16. C. Champin, M. Bellet, F. Schmidt, J.F. Agassant, Y. Le Maoult, PPS20. Akron, University of Akron. Paper 148. (2004)

NOMENCLATURE

r	Density (kg m^{-3})
c_p	Specific heat (J kg^{-1} K^{-1})
T	Temperature (K)
k	Thermal conductivity (W m^{-1} K^{-1})
$\overrightarrow{q_r}$	Density radiative heat flux (W m^{-2})
q_0	Initial density radiative heat fluxvalue (W m^{-2})
$\overline{A}$	Average absorption coefficient (m^{-1})
l	Distance covered inside the material (m)
$\vec{d}$	Ray direction
L	Radiation intensity (W m^{-2} sr^{-1})
S_W	Tungsten filament surface (m^2)
S_{Elt}	Element surface (m^2)
A_l	Spectral absorption coefficient (m^{-1})
L_l^0	Monochromatic radiation intensity of black body (W m^{-2} sr^{-1})
Δl	Spectral band (m)
$\underline{\underline{s}}$	Cauchy stress tensor (Pa)
$\underline{\underline{s}}'$	Cauchy extra stress tensor (Pa)
p'	Arbitrary pressure (Pa)
$\underline{\underline{I}}$	Identity tensor
$\underline{\underline{F}}$	Gradient tensor
C, a	Mooney-Rivlin first and second parameters
$\underline{\underline{B}}$	Cauchy-Green left tensor
$\underline{S}$	Stress vector (Pa)
$\underline{v}^*$	Virtual velocity (ms^{-1})
$\underline{\underline{\dot{e}}}^*$	Virtual strain rate tensor (s^{-1})
N_i	Interpolation function
Ω	Domain occupied by the material
x	Spatial coordinate (m)
v_i	i-th node velocity (m s^{-1})
ΔP	Pressure applied (Pa)
R	Internal radius (m)
S	External radius (m)